



Digital holographic microscopy for measurement of instantaneous contact angle of an evaporating droplet

Mohammad Mehdi Zamani Asl^{1,2} · Carlos A. Dorao¹ · Alberto Giacomello² · Maria Fernandino¹

Received: 15 June 2023 / Accepted: 14 August 2023 / Published online: 29 August 2023
© The Author(s) 2023

Abstract

Despite the apparent simplicity of the process of a droplet evaporating on a substrate, the temporal evolution of the local contact angle along the droplet periphery during the evaporation is still not fully understood. In this work, digital holographic microscopy is used for capturing the time evolution of the droplet surface at submicron resolution. The three-dimensional surface provides the information for determining the instantaneous three-phase contact line and the local apparent contact angle along the whole droplet periphery. The apparent contact angle is computed from the gradient of the droplet surface and defined as the maximum slope of this function along the periphery of the droplet. The method is then applied to study the diffusion dominated evaporation of nanoliter droplets on a hydrophilic substrate. For the case of a non-axisymmetric droplet, differences of up to 10° in contact angle along the contact line were identified when the contact line went from one pinning position to another. Digital holographic microscopy allowed us to characterize the irregular motion of the contact line and local changes in contact angle during the evaporation process.

1 Introduction

Droplet evaporation plays a significant role in various industrial applications ranging from coating (Erbil 2012; Gatapova et al 2018), spray cooling (Pautsch and Shedd 2005; Bhardwaj et al 2010) to inkjet printing (Yoo and Kim 2015). Due to this fact, droplet evaporation has been of major interest for researchers and has been studied intensively. Despite its apparent simplicity, there are many aspects of this phenomenon that are still unknown and need to be investigated in further detail. For instance, although the focus of research has generally been on evaporation of spherical droplets, local pinning and depinning of the contact line during the evaporation process results in non-spherical droplets with uneven three-phase contact lines. It has been widely recognized that the dynamics of the contact line, contact angle and local changes in curvature affect the

evaporation of droplets significantly (Brutin 2015; Orejon et al 2011).

Different modes of evaporation for sessile droplets have been identified based on the dynamics of the three-phase contact line (Moqaddam et al 2018). When the contact line is pinned, the droplet will evaporate in a constant contact radius mode (CCR) with a continuously decreasing contact angle. On the other hand, if the contact line is free to slide along the surface, a constant contact angle (CCA) evaporation mode will be observed. Since surfaces are never ideal or completely smooth, most of the time an alternate combination of these two modes is observed, usually referred to as stick–slip (SS) and stick-jump (SJ) modes (Debuissou et al 2016). The difference between these two is the faster retraction of the contact line as compared to the reduction in droplet height in the case of the latter, resulting in an abrupt change in droplet shape after the contact line jump (Dietrich et al 2015).

Due to the three-phase contact line dynamics and changes in the contact angle, the evaporation mode will strongly affect the mass flux from the liquid to the surrounding medium. The early study of Picknett and Bexon 1977 already showed that the mass of an evaporating droplet varies at a different rate for droplets in the CCR or CCA evaporating mode. Similar observations have been made by several authors after this (Hu and Larson 2002; Nguyen and

✉ Maria Fernandino
maria.fernandino@ntnu.no

¹ Department of Energy and Process Engineering, Norwegian University of Science and Technology, Kolbjørn Hejes v1b, 7491 Trondheim, Norway

² Department of Mechanical and Aerospace Engineering, Sapienza University of Rome, Eudossiana, 18, 00184 Rome, Italy

Nguyen 2012; Stauber et al 2014; Armstrong et al 2019). The effect of contact line dynamics on the droplet evaporation rate has also been investigated for the stick–slip (SS) and stick–jump (SJ) modes (Orejon et al 2011; Dietrich et al 2015). Surface wettability is another parameter determining the dynamics of sessile droplet evaporation Nguyen and Nguyen (2012), showing again the relevance of the contact angle in the evaporation process.

Although several previous studies of droplet evaporation have focused on spherical droplets, droplets do not always remain spherical and axi-symmetrical during the evaporation process, mainly due to the depinning of some portion of the contact line while the rest remains pinned. As it has been shown in the literature (Sáenz et al 2015, 2017), changes in the local curvature of a non-spherical droplet will affect the evaporation rate significantly, since the mass flux along the non-uniform contact line will vary locally. While local contact angle variations will lead to different local curvatures, the variations in contact angle will also influence the Marangoni flow inside the droplet, affecting the temperature and flow field and in the end the mass evaporation rate (Sáenz et al 2015, 2017).

Given that contact line dynamics, wettability and local curvature of the droplet along the three-phase contact line strongly affect the evaporation process of a sessile droplet, it becomes apparent that characterizing the local contact angle during the evaporation process is of vital importance to understand and predict droplet evaporation. The equilibrium contact angle θ_0 can be analytically expressed from the Young equation for ideally smooth surfaces as

$$\cos \theta_0 = \frac{\gamma_{SV} - \gamma_{SL}}{\gamma_{LV}} \quad (1)$$

with γ_{SL} and γ_{SV} the solid–vapor and solid–liquid interfacial energies and γ_{LV} the gas–liquid interfacial tension. However, surfaces are never ideally smooth or chemically homogeneous, and the resulting apparent contact angle θ varies from the one predicted here. In addition, the apparent contact angle is not unique and can vary between a minimum (receding contact angle) and a maximum (advancing contact angle) value. During dynamical processes such as droplet evaporation, the contact angle will vary dynamically between these two values.

There are currently several techniques available for measuring the apparent, advancing and receding contact angles with varying degrees of precision and accuracy. For the apparent contact angle, the most common approach is optical goniometry of a sessile droplet. Here, the contact angle is determined geometrically from a lateral image of the droplet. While this technique is simple and easy to implement, it has several limitations. First, the contact angle is measured only on two sides of the droplet, which

is not a valid approach if the droplet is non-axisymmetric. Secondly, it is sometimes difficult to determine the exact position of the three-phase contact line looking from the side of the droplet, especially for non-reflective surfaces, which introduces a big uncertainty in the measured contact angle from the geometrical fitting of the drop profile. Similarly, advancing and receding contact angles can be measured with optical goniometry with the tilting plate or liquid injection/retraction methods or the Wilhelmy plate method. The limitations of these methods lie again in the uncertainty introduced when determining the position of the contact line geometrically and on the fact that the contact angles are measured only at two opposing points of the droplet lateral image.

There are some techniques that can overcome the limitation of two-point contact angle measurements by measuring the contact angle at every point along the three-phase contact line. One of them is an optical reflection-refraction method proposed by Allain et al (1985), useful for the measurement of low contact angles. The technique is limited to liquids and surfaces with a certain amount of reflectance. A similar laser shadowgraphy method was later proposed by Zhang and Chao (2002), capable of measuring the dynamic contact angle of a sessile droplet on a nontransparent metal substrate while simultaneously visualizing the flow motion inside the droplet. The contact angle can be obtained from solving two equations involving the refracted angle from the liquid and some geometrical parameters of the optical system.

Another more attractive technique that has been used to measure the contact angle along the whole droplet periphery is confocal microscopy (Sundberg et al 2007; Chesna et al 2016). The main advantage of this technique compared to traditional goniometry is that the droplet can be measured from above, which eliminates the complexities of identifying the triple-phase contact line when viewed from an oblique angle. This technique is reported to be suitable for measuring both low ($<30^\circ$) and relatively high contact angles ($30^\circ - 90^\circ$) (Sundberg et al. 2007). One limitation of confocal microscopy for the study of dynamic contact angle evolution is its time resolution limited by the acquisition speed. With frame rates in the order of some frames per second, this technique requires a certain time to reconstruct the image of the droplet, time that can be much larger than the characteristic time evolution of a fast evaporating droplet. In addition, confocal microscopy involves the use of fluorescence particles or dye for visualization. Recently, Gatapova et al (2018) used a shadow and image-analyzing interference technique to measure contact angles during the final stage of a droplet evaporation. The method consisted in finding the height profile of the droplet and calculating the contact angle by assuming a spherical cap and finding the tangent to the circle close to the surface.

Here, we use digital holographic microscopy (DHM) (Kim 2014) for the instantaneous characterization of the contact angle along the whole contact line periphery of an evaporating droplet. Digital holographic microscopy is an advanced technique which combines the digital holography principle with microscopy in order to study microscopic samples and reconstruct the 3D holograms. Contrary to confocal microscopy, DHM does not need the vertical mechanical movement to reconstruct the 3D images, allowing for a fast scanning of the object of interest. With a 3D holographic image of the object available, all relevant information such as contact angle, surface curvatures and contact line motion can be obtained. Although the technique has been around for decades, its main use has been in the field of life sciences for the observation of cells and cellular processes (Katz and Sheng 2010; Rappaz et al. 2010) and in material sciences for the characterization of surfaces and defects (Colomb 2011). The application of this DHM technique in the field of fluid mechanics has been rather scarce, namely for following 3D trajectories of tracer particles inside a confined droplet (Lee et al. 2014), for the Lagrangian tracking of particles and their evaporation rate in a turbulent flow (Marié et al. 2017), and very recently for the observation of capillary waves on a droplet surface under acoustic actuation (Zhang et al. 2023).

In this work, we use digital holographic microscopy to characterize the temporal evolution of the three-phase contact line during evaporation of a nano-liter droplet on a hydrophilic surface. This technique allows us to have an instantaneous description of the contact angle along the whole droplet periphery simultaneously. We compare the evaporation and contact line dynamics of an axisymmetric and a non-axisymmetric evaporating droplet, focusing on the stick and slip motion of the contact line and consequent local variations of contact angle.

2 Experimental setup and methods

2.1 Materials

Droplet evaporation experiments were performed over wafers of 500 mm thick lithium niobate ($LiNbO_3$). This transparent substrate was chosen before glass due to a larger static contact angle as compared to the latter.

The substrate was cleaned first with ethanol, followed by isopropanol and dried with nitrogen gas. With this cleaning procedure, little or no contact line pinning was observed during the droplet evaporation process. To induce contact line pinning and the occurrence of constant contact base evaporation mode, the sample was washed with tap water. This procedure leaves organic residues that help pin the contact line.

Deionized (DI) water was used as fluid for the generated droplets. Droplets were generated by a Pipe Jet-P9 Nano Dispenser from BioFluidix Co. with an S200 Pipe tip to generate 12 nanoliter droplets, way below the capillary length where gravitational effects become relevant.

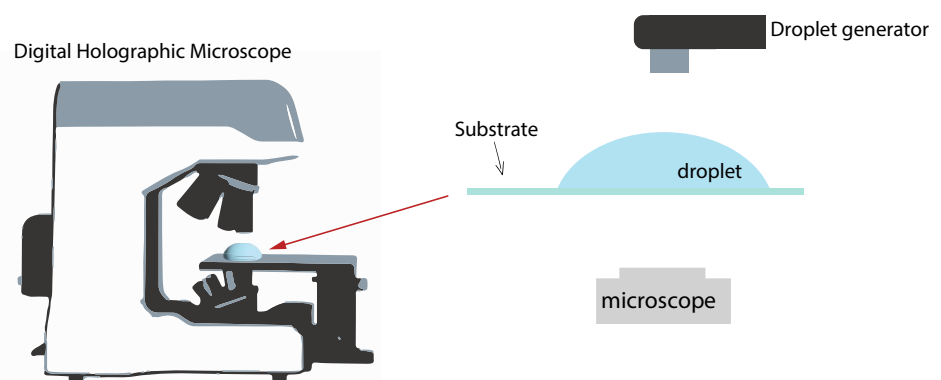
The evolution of the evaporating droplet was visualized by a transmission T-1000 digital holographic microscope from Lyncée Tec AS. A 10X objective was used for these experiments, giving a spatial resolution of $15\mu m$ and a field of view of $660 \times 660 \mu m^2$. Images were obtained at a rate of 15 fps, giving a temporal resolution of 66ms.

2.2 Experimental setup and procedure

A schematic representation of the experimental setup is shown in Fig. 1. The setup consisted of the $LiNbO_3$ substrate placed on a microscope stage. The nano-dispenser was placed over the surface until the droplet generation. The droplet was released from a height of 3 cm above the sample.

Evaporation experiments were performed at open conditions, with a relative humidity of 17% and ambient temperature of $24^\circ C$. The substrate was kept at ambient temperature,

Fig. 1 Experimental setup used for this work, consisting of a transmission digital holographic microscope, a hydrophilic substrate and a nano-liter droplet dispenser. The sample was placed on the DHM stage. A water droplet was deposited on the substrate with the nano-liter dispenser. The dispenser was moved away from under the microscope immediately after the droplet deposition. Acquisition with the DHM started 15 s after deposition



so that the droplet evaporation was in the diffusion dominated regime.

After deposition of a droplet, the nano-dispenser was moved to the side to allow for a free visual path from the microscope objective. This process took around 15 s before we started recording images. This allowed for the droplet to go over the initial settling transient after deposition. Also, due to evaporation of the droplet, its size became small enough to enter fully into our field of view. All experiments were performed in the same systematic way, where acquisition of images with the DHM was started 15 s after deposition of the droplet.

Images were recorded with a speed of 15 fps during the droplet lifetime. The images obtained from the DHM microscope were analyzed with an in-house developed script in MATLAB. Given the field of view of our optical system, only droplets of less than 660 μm in diameter could be observed wholly in our system.

2.3 Contact angle from DHM images

Contrary to the traditional approach of obtaining the contact angle of a droplet using shadowgraphy from a lateral view of the droplet, the use of digital holographic microscopy (DHM) allow us to obtain a 3D representation of the droplet. While with confocal microscopy a series of images need to be acquired for one 3D imaging of the droplet, DHM obtains a 3D representation in one exposure, which is a significant advantage for the study of contact angle variation during fast dynamic processes such as nano droplet evaporation. Based on this instantaneous three-dimensional representation of the droplet, one can obtain the information of the contact line shape and contact angle all along the periphery of the droplet at the same time. The main limitation in temporal resolution is given by speed of the camera used.

Digital holographic microscopy (DHM) works in a similar way as holography by using two coherent beams, namely one beam (reference beam) used as reference and the other one going through the object (object beam) of interest, resulting in the formation of an interference pattern. In DHM, the phase shift in the object beam, instead of its intensity, is registered digitally so that the hologram with all the information about the illuminated object is available. The registered hologram is then processed by software to reconstruct the 3D image of the object, removing the necessity of a mechanical scan of the sample. Both reflection and transmission configurations can be used in DHM. In this work, we use a transmission T-1000 digital holographic microscope from Lyncée Tec AS. In this configuration, a single beam is split into a reference and an object beam. The transmitted object beam is collected by the objective of the microscope and then recombined with the reference beam to form a hologram in the camera. The dephasing $\Delta\varphi$

is used to recover the 3D topology of the object as (Lyncée Tec SA 2022)

$$\Delta h = \frac{\lambda \Delta \varphi}{2\pi(n_2 - n_1)} \quad (2)$$

where Δh , λ , $\Delta\varphi$, n_2 , and n_1 are the sample height, beam dephasing, beam wavelength, refraction index of the liquid sample, and refraction index of medium, respectively.

One limitation of transmission DHM for contact angle measurement is that only hydrophilic cases can be considered. This is because of the way DHM works, namely the difference in light path between the reference and object beams. In the case of a droplet on a hydrophobic surface, i.e., contact angle larger than 90° , the light from the object beam needs to go through liquid and air again below the droplet before reaching the objective. The processing of the resulting dephasing of the object beam cannot distinguish between this discontinuity in the fluid medium. On the other hand, due to the high vertical spatial resolution, DHM allows for measurement of very low contact angles, which is usually a challenge for the other traditional techniques. Another limitation also inherent to all optical systems, is the fact that the visualization of a droplet, especially close to the contact line region, is limited by the amount of light scattered from the surface and coming into the optical system. A too high contact angle will simply result in dark regions in the images, since light will be directed outside of the receiving optics. In our case, we have used a 10X objective with a numerical aperture of 0.32. The maximum contact angle that we could resolve was approximately 40° . One way of allowing for a larger field of view and therefore the ability to visualize whole, larger droplets, would have been to use an objective of lower magnification. However, a smaller magnification also implies a smaller numerical aperture, which decreases the maximum contact angle that can be measured by the system. In our case, going to an objective of 5X or 2.5X would have allowed for the visualisation of a larger droplet, but only contact angles smaller than 19° and 10° , respectively, could have been measured. For this reason, it was decided to stay with the 10X objective instead of restricting the study to small contact angles. After all, droplets as small as the ones used in this study are always present during the last stages of evaporation of larger droplets, making this study relevant for larger droplets as well.

The instantaneous contact angle along the whole contact line length was obtained from the analysis of the 3D images obtained from the DHM microscope. An example of these images is shown in Fig. 2, where a 3D reconstruction of the whole droplet surface is observed. The contact angle can be determined from the gradient of the droplet height profile $\Gamma(x, y)$ obtained from the DHM and shown in Fig. 2a. The gradient indicates the change in slope of the droplet surface.

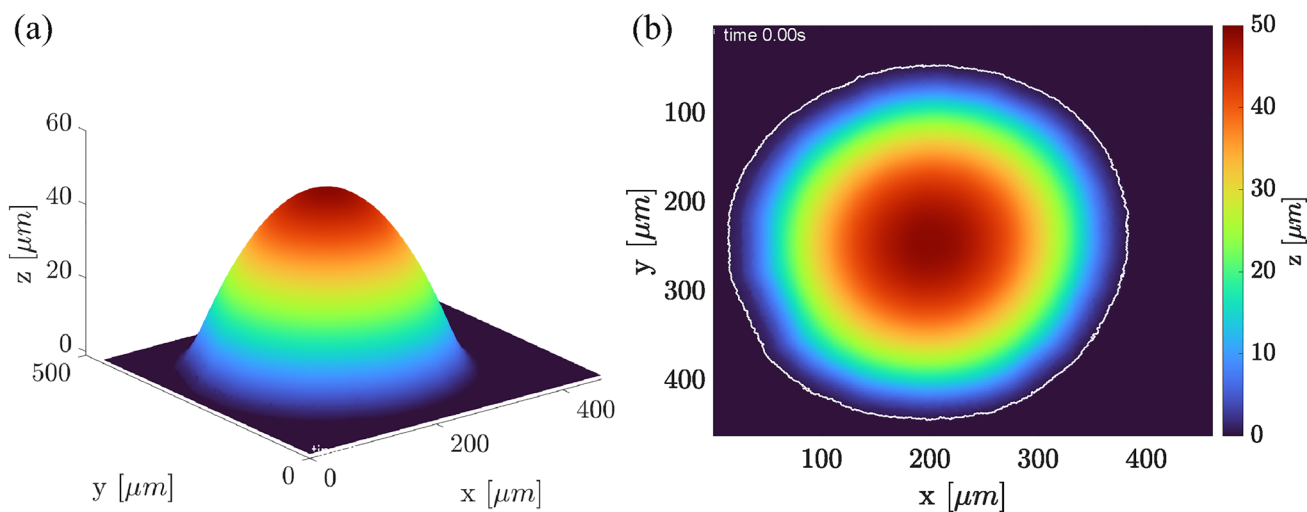


Fig. 2 Digital holographic microscopy image of a nanoliter droplet: **a** droplet height profile from 3D droplet surface reconstruction; **b** top view of the droplet surface

The norm of the gradient of the height profile in Fig. 2a, calculated as

$$\phi = \sqrt{\left(\frac{\partial \Gamma}{\partial x}\right)^2 + \left(\frac{\partial \Gamma}{\partial y}\right)^2} \tag{3}$$

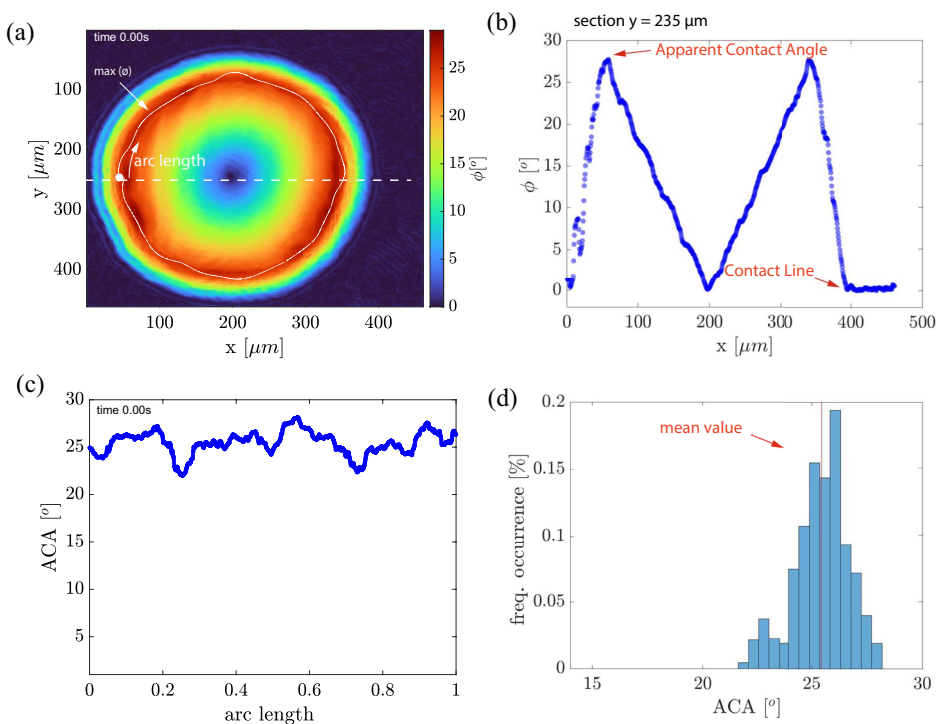
can be seen in Fig. 3a with its corresponding centerline cut in Fig. 3b. The contact angle is then obtained from the gradient as

$$\theta = \max\{\arctan(\phi)\} \tag{4}$$

The reason for the maximum in Eq. 4 is explained below.

Figure 3b shows that the gradient goes from zero towards an increasing value once the droplet is reached. This line represents the three-phase contact line. The three-phase contact line location will depend on the vertical resolution of the DHM microscope. In our case, this vertical resolution is specified to be 2nm. Once inside the three-phase contact

Fig. 3 Images showing the post-processing procedure to obtain the contact angle from the DHM images. **a** Gradient of the droplet height profile from Fig. 2 as obtained with Eq. 4. The white contour represents the group of points at the maxima in figure (b). **b** Profile of the gradient along the dash line in figure (a). The contact line is defined at the points where the gradient goes from zero to a positive value. The apparent contact angle is defined on the maxima of the gradient representing the points of maximum slope and inflection point in the surface curvature. **c** Apparent contact angle along the white contour around the droplet perimeter (normalized arc length). **d** Histogram of the apparent contact angle values in figure (c)



line, the gradient grows fast towards a maximum value. These points of maximum value indicate the region or line with maximum change in slope or the inflection point in surface curvature. Since these points represent the closed line with higher curvature change, this contour can be interpreted as the apparent contact angle which lies approximately 50 micrometers inside the three-phase contact line, and corresponding in this case to a droplet surface height of around $10\ \mu\text{m}$. From this maximum value, the norm of the gradient decreases smoothly and monotonously until the center of the droplet where it recovers a zero value. Note that in Fig. 3b, there is a local maximum before reaching the global maximum defining the apparent contact angle. This local maximum comes from the fluctuations that appear after obtaining the plots in Fig. 3a, b from the derivative of the droplet surface height in Fig. 2. These fluctuations are purely numerical and the local maximum has no physical meaning.

The instantaneous apparent contact angle along the normalized arc length of the droplet perimeter is shown in Fig. 3c, with a mean value of 25° and a variation of up to 4 degrees at different points along the contact line, as also shown in the histogram in Fig. 3d.

To verify this definition of the apparent contact angle, we performed a geometrical fitting of a circle on the nano-liter droplet image, as shown in Fig. 4. The contact angle obtained from the extrapolation of this curve from the liquid to the solid surface predicts a contact angle of 23.8° , similar to our definition of the apparent contact angle obtained from the DHM images.

Because now we have information of the surface of the droplet at all times, we can get the values of the contact

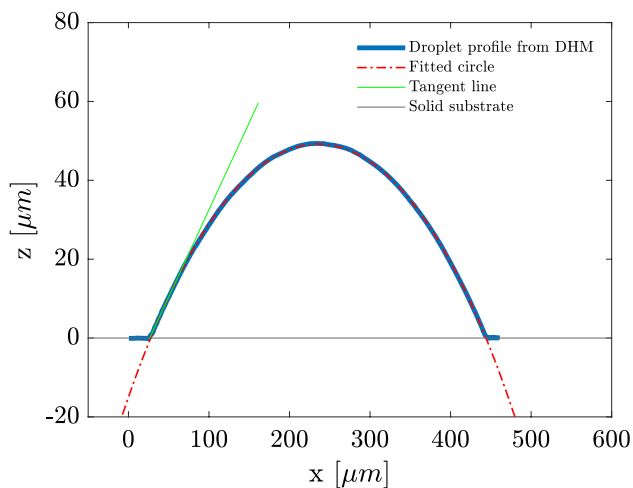


Fig. 4 Geometrical fit of a circle on the nano-liter droplet from Figs. 2 and 3. The tangent of the circle at the three-phase contact point indicates a contact angle of 23.8° , showing with good agreement with the apparent contact angle as defined from the DHM images

angle instantaneously and locally along the periphery of the droplet, both for spherical and non-axisymmetric droplets. In the next section, experiments during droplet evaporation show how the contact angle can change significantly along the contact line, also correlated by the stick, jump and slip motion of the moving three-phase contact line.

3 Results and discussions

Droplet evaporation in the diffusion dominated regime was studied under the conditions and with the techniques described above. The results obtained for two cases are shown here, namely evaporation of an axi-symmetric droplet showing a constant contact angle (CCA) evaporation mode, and a non-axisymmetric droplet with initial constant contact base (CCB) evaporation mode, followed by stick–slip (SS) and stick-jump (SJ) motions.

3.1 Axi-symmetric evaporating droplet

Figure 5a shows the time evolution of the contours of an evaporating droplet, where the droplet shape remains approximately axi-symmetric during the whole evaporation process. The time lapse between each contour line is 263ms, with a total evaporation time for the droplet of around 10.5s from the time the image acquisition started. Figure 5b shows the corresponding contact angle along the droplet periphery at different times.

The droplet in Fig. 5 evaporates nearly in a CCA mode, where there is little pinning and continuous motion of the three-phase contact line with no clear observable jump in the motion. Although there is some relatively higher pinning of the triple contact line in some portions of the line, the base diameter of the droplet decreases rather uniformly from all sides. Figure 5b shows that at each time, the contact angle along the droplet periphery has a relatively constant value with a maximum variation of $\pm 3^\circ$. During the first 6 s of the recorded evaporation, the contact angle remains constant, indicating a CCA evaporation mode. After approximately 7 s into the evaporation process, larger jumps in contact angle value along the droplet periphery are observed (yellow curve in Fig. 5b), reaching up to 8° in difference between different points. The larger difference happens around the region of less movement of the contact line, indicating the occurrence of some pinning. After this and once the droplet reaches a certain size and height, the contact angle decreases fast while maintaining a constant value at all points along the droplet periphery, until total evaporation of the droplet.

A mean contact angle around the droplet can be defined as

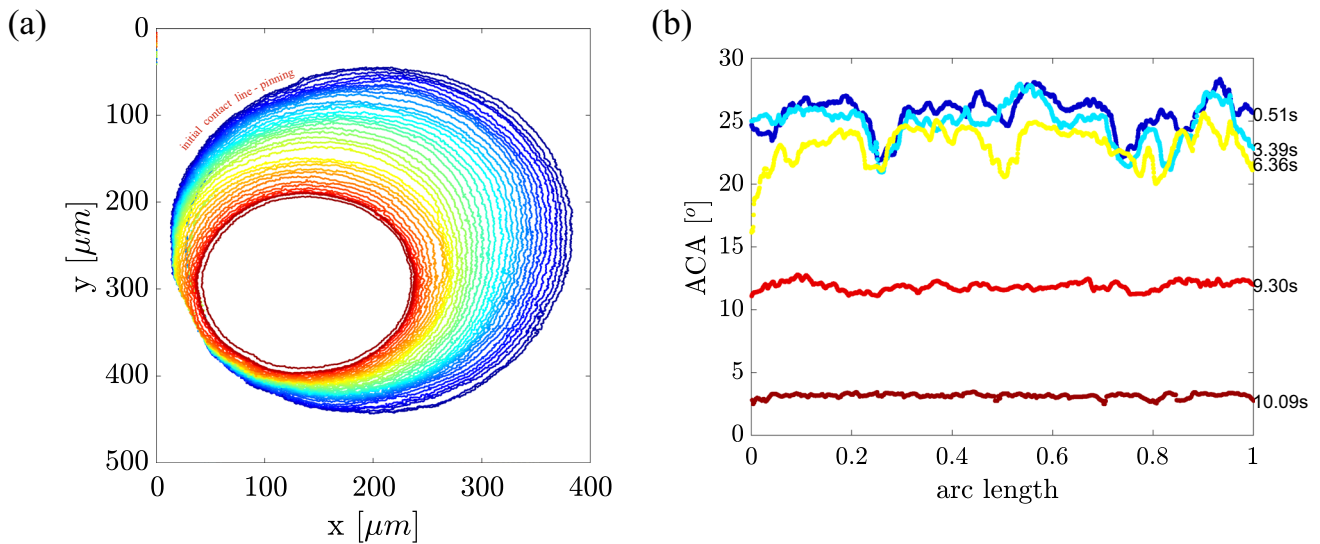


Fig. 5 Evaporation of axi-symmetric droplet undergoing CCA evaporation mode. **a** Time evolution of droplet contour during the evaporation process. **b** Apparent contact angle along the droplet periphery

(normalized arc length) at different times. The colors of the contact angles shown in **(b)** correspond to the colors of the contours in **(a)**

$$\bar{\theta} = \frac{1}{N} \sum_{i=1}^N (\theta_i) \tag{5}$$

where θ_i is the value of local contact angle at each point on the contact line, and N is the number of elements of the local contact angle vector. The time evolution of the mean contact angle for this axi-symmetric droplet is seen in Fig. 8, also compared to the mean contact angle of the non-axisymmetric droplet to be discussed in the next section. Looking for now at the CCA evaporation mode of the axi-symmetric

droplet, one can see that indeed the mean contact angle remains constant until around 7 s into the evaporation process showing a fast decreases in the last stages of the evaporation. At this point, the droplet is flat enough so that the line tension dominates, driving the contact line towards the droplet center very fast.

The evolution of the droplet height and base diameter during the evaporation is seen in Fig. 6. The droplet height decreases monotonically, with a much higher speed during the last 2 s before the droplet is totally evaporated. Just before these last 2 s, the droplet height is around 25 μm

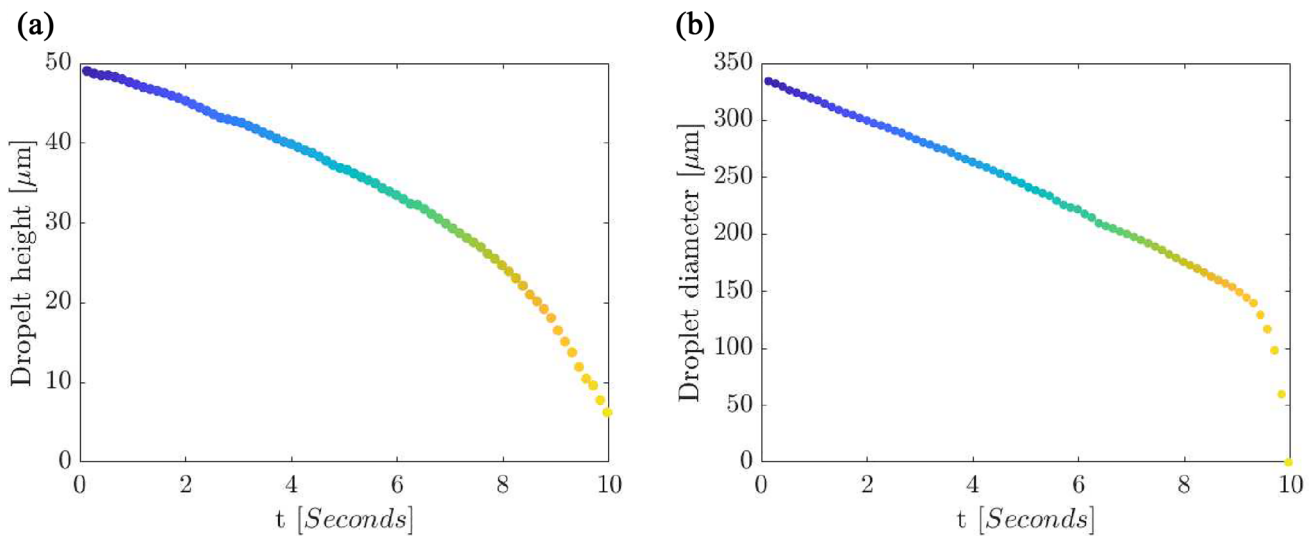


Fig. 6 Time evolution of **a** height and **b** diameter of axi-symmetric droplet evaporating in CCA evaporation mode

while its diameter is more than $150\ \mu\text{m}$. This shows that the droplet actually resembles more a liquid film during the last stages of evaporation. At a little over 9 s, the three-phase contact line is depinned, pulled inwards and the droplet diameter shows a fast decrease towards zero until full evaporation. This phenomenon of contact line depinning and sudden increase in contact line velocity has been referred to as stage IV in the droplet evaporation process in the literature (Bourges-Monnier and Shanahan 1995; Gatapova et al. 2018). Interestingly, the droplet height when this last stage is observed in our study lies between 13 and $14\ \mu\text{m}$, same value as reported by Gatapova et al. (2018) for droplets evaporating on different substrates.

3.2 Non-axisymmetric evaporating droplet

While a droplet evaporating in CCA mode showed a uniform contact angle around the droplet periphery for each time, a droplet whose triple-contact line pins and depins intermittently can be expected to have different contact angle values at different points of the contact line. As explained in Sect. 2, in order to induce contact line pinning, the samples were additionally washed with tap water. In this way, the organic residues left after the washing helped pin the contact line and the CCB evaporation mode could be observed.

Figure 7 shows the time evolution of an evaporating droplet undergoing intermittent pinning and depinning of the three-phase contact line. The droplet in Fig. 7a shows an initial evaporation at CCB mode. The time lapse between each contour line is 263 milliseconds, showing that the droplet remains pinned at all points during the first 2.7 s of the evaporation. Looking at Fig. 7b, it can be seen that during this pinned period (blue line) the contact angle is approximately

uniform along the whole droplet periphery, with fluctuations around ± 2 degrees. While the droplet evaporates in this mode and the contact angle decreases, the net capillary force pulling the contact line inwards becomes more and more horizontal. After a certain contact angle has been reached, the line tension pulling the contact line inwards is large enough to overcome the energy barrier to depin the contact line, although this does not happen at every point of the contact line. At this point, the part of the contact line that depins moves fast until it reaches a new position where it is pinned again. This stick-jump (SJ) process takes less than 100 milliseconds.

Just after the new pinning occurs, the contact angle along the whole triple contact line increases significantly as seen in Fig. 7b, even at places where the contact line has remained pinned. This is because in this short time during the transition, the droplet volume does not change significantly, and capillary forces take the droplet to a new equilibrium shape corresponding to the same liquid volume in a smaller base area. This is referred to as a stick-jump (SJ) motion. Note that after the jump, the contact angle is no longer uniform along the contact line, with more than 10 degrees difference between several points along the droplet periphery. The minima of contact angle values observed in Fig. 7b correspond to points where the contact line is moving, i.e., regions of no contact line pinning.

Even with the large fluctuations in contact angle observed after the first contact line jump, the contact angle profile remains relatively unchanged for around 7 s during the evaporation process. During this period, the droplet evaporates in a combined CCA and CCB mode, with intermittent pinning and depinning of the contact line, as better observed from Fig. 8 for the SS case between 2.5 sec and 10 sec. The

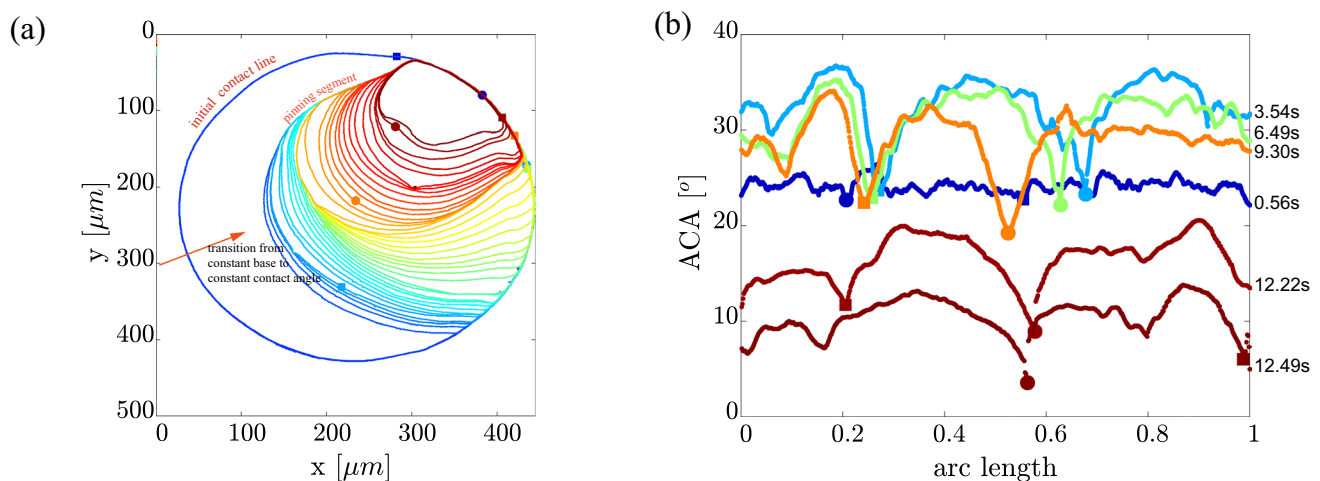


Fig. 7 Evaporation process of a nanoliter droplet in alternating CCB and CCA modes: **a** time evolution of droplet contours; **b** time evolution of local contact angle along the droplet periphery (normalized

arc length). The large dots on the contact angle along the arc length correspond to the positions indicated by corresponding dots on the droplet contours

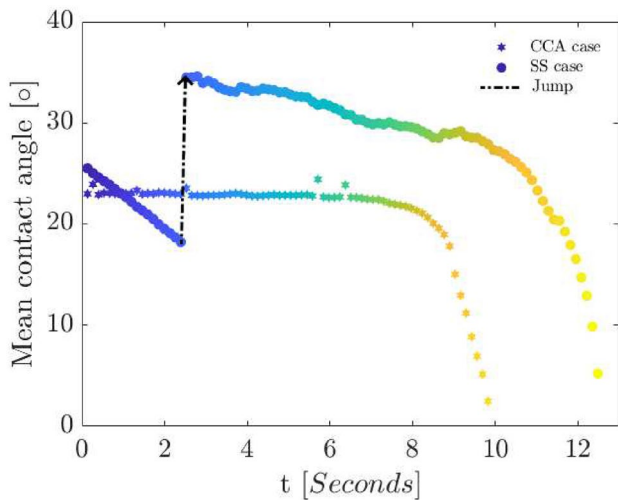


Fig. 8 Mean contact angle (Eq. 5) temporal evolution for the axisymmetric (CCA) and non-axisymmetric (SS) droplets from Figs. 5, 6, and 7, respectively. The axisymmetric droplet shows a constant contact angle (CCA) evaporation mode while the non-axisymmetric droplet shows one stick-jump (SJ) motion followed by a stick-slip (SS) evaporation mode

figure shows the initial evaporation stage when the three-phase contact line remains pinned and the contact angle decreases monotonously during the first 2.5 s. After the SJ motion, the mean contact angle increases. For the following 7 s, the mean contact angle decreases in finite steps, indicating a stick-slip (SS) motion during this stage. When the droplet reaches a critical height, the three-phase contact line is depinned and the droplet evaporates completely relatively fast. The last stage of evaporation seems to be faster for the case of the CCA droplet than for the SS one, probably due to

the extra pinning-depinning occurrences takes place for the latter. This can be confirmed by looking at the contact angle along the droplet arc length in Fig. 7b for the last two dark red curves (corresponding to 12.22sec and 12.24sec). As it can be seen from here and from the corresponding droplet contours in Fig. 7a, the droplet remains non-axisymmetric also during the last stage of evaporation, showing a large variation of local contact angle along its periphery, indicating local three-phase contact line pinning at various points.

Figure 9 shows the temporal evolution of the droplet height and base diameter for the droplet shown in Fig. 7. After the first SJ motion, there is a significant increase in the droplet height due to the fast change in contact line position and the new equilibrium shape for the droplet. At the same time, the droplet diameter jumps to a lower value. After this strong SJ motion, the droplet continues to evaporate in a mixed SS mode, where small jumps in droplet height can be observed, corresponding to local contact line depinning events. Same as for the axisymmetric droplet in the previous section, the droplet diameter decreases at a much faster rate than the droplet height during the last stage of evaporation, indicating that the droplet is more similar to a thin liquid film before evaporating completely.

4 Conclusions

In this work, we have shown the use of digital holographic microscopy (DHM) for determining the instantaneous local contact angle around the whole periphery of an evaporating nanoliter droplet. By using DHM, we have full information about the droplet surface and shape. By taking the gradient of the obtained droplet surface, we were able to identify the

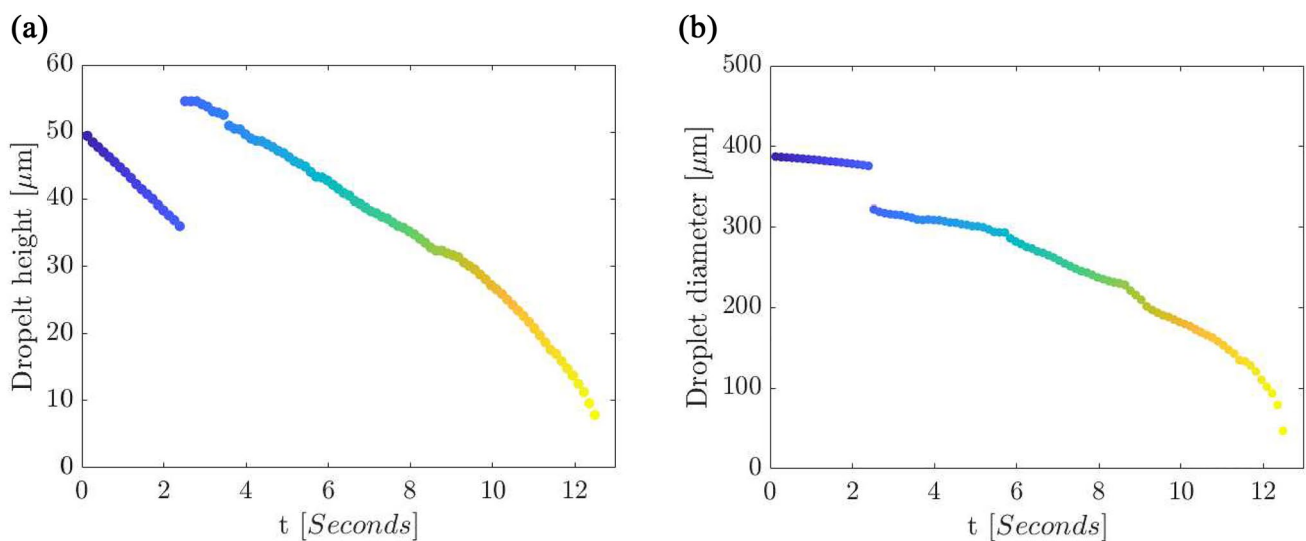


Fig. 9 Time evolution of **a** height and **b** diameter of alternating CCA and CCB evaporation modes

three-phase contact line, namely where the surface gradient becomes non-negative, and the apparent contact angle, corresponding to the points of maximum change in surface slope. This new identification of the apparent contact angle located only a few micrometers from the three-phase contact line was possible thanks to the higher spatial resolution in the DHM as compared to other traditional optical methods to measure contact angle. To demonstrate this technique, we studied the diffusion dominated evaporation of nanoliter droplets. We were able to identify regions along the contact line with more than 10 degrees difference in contact angle when the three-phase contact line went from one pinning position to another during the CCB evaporation mode. The characterization of the difference in contact angle from point to point along the contact line and the fast and irregular motion of the contact line was possible thanks to the DHM technique used in this work. Digital holographic microscopy is a promising technique that presents several advantages over other traditional optical techniques for studying contact line and contact angle dynamics.

Acknowledgments Funding for this work from the Research Council of Norway under FRIPRO Project No. 275587 is gratefully acknowledged.

Author contributions Conceptualization and methodology were contributed by MMZA, CAD, MF; experiments and analysis were contributed by MMZA, CAD, MF; discussions were contributed by MMZA, CAD, AG, MF; writing—original draft preparation, was contributed by MMZA, MF; writing—review and editing, was contributed by MMZA, CAD, AG, MF; funding acquisition was contributed by MF; supervision was contributed by CAD, AG, MF.

Funding Open access funding provided by NTNU Norwegian University of Science and Technology (incl St. Olavs Hospital - Trondheim University Hospital). Funding for MF for this work from the Research Council of Norway, FRIPRO Project No. 275587.

Availability of data and materials All data from this study are available from the corresponding author on reasonable request.

Declarations

Conflict of interest The authors declare no conflict of interest.

Ethical Approval Not applicable.

Open Access This article is licensed under a Creative Commons Attribution 4.0 International License, which permits use, sharing, adaptation, distribution and reproduction in any medium or format, as long as you give appropriate credit to the original author(s) and the source, provide a link to the Creative Commons licence, and indicate if changes were made. The images or other third party material in this article are included in the article's Creative Commons licence, unless indicated otherwise in a credit line to the material. If material is not included in the article's Creative Commons licence and your intended use is not permitted by statutory regulation or exceeds the permitted use, you will need to obtain permission directly from the copyright holder. To view a copy of this licence, visit <http://creativecommons.org/licenses/by/4.0/>.

References

- Allain C, Aussere D, Rondelez F (1985) A new method for contact-angle measurements of sessile drops. *J Colloid Interface Sci* 107(1):5–13
- Armstrong S, McHale G, Ledesma-Aguilar R et al (2019) Pinning-free evaporation of sessile droplets of water from solid surfaces. *Langmuir* 35(8):2989–2996
- Bhardwaj R, Longtin JP, Attinger D (2010) Interfacial temperature measurements, high-speed visualization and finite-element simulations of droplet impact and evaporation on a solid surface. *Int J Heat Mass Transf* 53:3733–3744
- Bourges-Monnier C, Shanahan MER (1995) Influence of evaporation on contact angle. *Langmuir* 11:2820–2829
- Brutin D (ed) (2015) *Droplet wetting and evaporation*. Academic Press, Elsevier, Aix-Marseille University, Marseille, France
- Chesna JW, Wiedmaier BF, Wang J et al (2016) Aerial wetting contact angle measurement using confocal microscopy. *Meas Sci Technol* 27(125):202
- Colomb KJT (2011) Digital holographic microscopy. In: Leach R (ed) *Optical measurement of surface topography*. Springer, New York
- Debuisson D, Merlen A, Senez V et al (2016) Stick-jump (sj) evaporation of strongly pinned nanoliter volume sessile water droplets on quick drying, micropatterned surfaces. *Langmuir* 32(11):2679–2686
- Dietrich E, Kooij ES, Zhang X et al (2015) Stick-jump mode in surface droplet dissolution. *Langmuir* 31(16):4696–4703
- Erbil HY (2012) Evaporation of pure liquid sessile and spherical suspended drops: a review. *Adv Colloid Interface Sci* 170:67–86
- Gatapova EY, Shonina AM, Safonov AI et al (2018) Evaporation dynamics of a sessile droplet on glass surfaces with fluoropolymer coatings: focusing on the final stage of thin droplet evaporation. *Soft Matter* 14:1811–1821
- Hu H, Larson RG (2002) Evaporation of a sessile droplet on a substrate. *J Phys Chem B* 106:1334–1344
- Katz J, Sheng J (2010) Applications of holography in fluid mechanics and particle dynamics. *Annu Rev Fluid Mech* 42:531–555
- Kim MK (2014) Principles and techniques of digital holographic microscopy. *SPIE Rev* 17(1):80–88
- Lee SJ, Hong J, Choi YS (2014) Evaporation-induced flows inside a confined droplet of diluted saline solution. *Langmuir* 30:7710–7715
- Lyncée Tec SA (2022) *Software Koala V8.2, User operating manual*. Innovation Park, Building PSE A, Lausanne
- Marié JL, Tronchin T, Grosjean N, et al (2017) Digital holographic measurement of the Lagrangian evaporation rate of droplets dispersing in a homogeneous isotropic turbulence. *Exp Fluids* 58(11)
- Moqaddam AM, Derome D, Carmeliet J (2018) Dynamics of contact line pinning and depinning of droplets evaporating on microribs. *Langmuir* 34:5635–5645
- Nguyen TAH, Nguyen AV (2012) On the lifetime of evaporating sessile droplets. *Langmuir* 28:1924–1930
- Oregon D, Sefiane K, Shanahan MER (2011) Stick-slip of evaporating droplets: Substrate hydrophobicity and nanoparticle concentration. *Langmuir* 27(21):12834–12843
- Pautsch AG, Shedd TA (2005) Spray impingement cooling with single- and multiple-nozzle arrays. Part I: heat transfer data using FC-72. *Int J Heat Mass Transf* 48:3167–3175
- Picknett RG, Bexon R (1977) The evaporation of sessile or pendant drops in still air. *J Colloid Interface Sci* 61(2):336–350
- Rappaz B, Breton B, Shaffer E et al (2010) Digital holographic microscopy: a quantitative label-free microscopy technique for phenotypic screening. *Combin Chem High Throughput Screen* 17(018):005

- Sáenz PJ, Sefiane K, Kim J et al (2015) Evaporation of sessile drops: a three-dimensional approach. *J Fluid Mech* 772:705–739
- Sáenz PJ, Wray AW, Che Z et al (2017) Dynamics and universal scaling law in geometrically-controlled sessile drop evaporation. *Nat Commun* 8(14):783
- Stauber JM, Wilson SK, Duffy BR et al (2014) On the lifetimes of evaporating droplets. *J Fluid Mech* 744:R2
- Sundberg M, Månsson A, Tågerud S (2007) Contact angle measurements by confocal microscopy for non-destructive microscale surface characterization. *J Colloid Interface Sci* 313:454–460
- Yoo H, Kim C (2015) Experimental studies on formation, spreading and drying of inkjet drop of colloidal suspensions. *Colloids Surf A Physicochem Eng Aspects* 468:234–245
- Zhang N, Chao DF (2002) A new laser shadowgraphy method for measurements of dynamic contact angle and simultaneous flow visualization in a sessile drop. *Opt Laser Technol* 34(3):243–248
- Zhang S, Orosco J, Friend J (2023) Onset of visible capillary waves from high-frequency acoustic excitation. *Langmuir* 39(10):3699–3709

Publisher's Note Springer Nature remains neutral with regard to jurisdictional claims in published maps and institutional affiliations.